Journal of Applied Pharmaceutical Science Vol. 14(06), pp 147-153, June, 2024
Available online at http://www.japsonline.com
DOI: 10.7324/JAPS.2024.169961
ISSN 2231-3354

# Green precipitation method using *Polyscias scutellaria* extract in the synthesis of hydroxyapatite/alginate/copper (II) oxide composites as a drug carrier

Wulandari Wulandari, Novesar Jamarun*, Diana Vanda Wellia, Emriadi Emriadi
Department of Chemistry, Faculty of Mathematics and Natural Sciences, Universitas Andalas, Padang, 25163, Indonesia.

**ARTICLE HISTORY**
Received on: 18/01/2024
Accepted on: 14/04/2024
Available Online: 05/06/2024

***Key words:***
Composite, hydroxyapatite, alginate, drug carrier, antibacterial.

**ABSTRACT**

Hydroxyapatite (HAp) is a bioceramic naturally present in human bones and teeth, prized for its exceptional biocompatibility, bioactivity, and capacity for osteointegration, rendering it a viable candidate for biomedical applications as a drug delivery system. Nevertheless, HAp possesses limited antibacterial properties. Thus, the present study focuses on synthesizing HAp/alginate/copper oxide (HAp/Alg/CuO) composite to augment these attributes. An environmentally friendly synthesis approach is explored to create the HAp/Alg/CuO composite. *Polyscias scutellaria* leaf extract is anticipated to function as a capping agent, facilitating control over the composite's morphology. In addition, residual bamboo clam shells serve as the precursor material for HAp fabrication. The composites prepared were analyzed by a series of characterization techniques such as X-ray diffraction (XRD), Fourier transform infrared spectroscopy (FTIR), and scanning electron microscopy-energy dispersive spectroscopy (SEM-EDS). XRD analysis revealed the formation of HAp/Alg/CuO composites exhibiting a hexagonal structure consistent with the ICSD (The inorganic Crystal Structure Database) #157481 standard. The crystallite size was obtained at 30.00, 33.35, 24.14, and 26.84 nm for HAp/Alg/CuO-1, HAp/Alg/CuO-2, HAp/Alg/CuO-3, and HAp/Alg/CuO-4, respectively. FTIR analysis confirmed the presence of the hydroxyl, phosphate, carboxylic, and metal-oxide (Cu–O) bonds. SEM images revealed irregularly shaped, agglomerated particles with an average particle size of 0.416 µm. EDS spectra exhibited calcium, carbon, phosphorus, and oxygen elements. Clindamycin-loaded HAp/Alg/CuO composites were assessed for their antibacterial efficacy against Gram-positive *Staphylococcus aureus* and Gram-negative *Escherichia coli* bacteria. The inhibition zones observed suggest that clindamycin-loaded HAp/Alg/CuO composites hold promise as drug delivery vehicles. Further investigation and development of these composites are warranted, with potential applications in treating specific ailments attributed to *S. aureus* and *E. coli* infections, such as osteomyelitis.

## INTRODUCTION

Hydroxyapatite (HAp), also known as $Ca_{10}(PO_4)_6(OH)_2$, is a primary inorganic composition of human bone and teeth [1]. It is one of the most alluring biomaterials utilized for bone implants due to its biological and chemical similarity to human tissue [2,3]. In addition to having a high degree of biocompatibility, HAp also has excellence in bioactivity and the capacity to attach to bone directly, which promotes effective osteointegration. HAp is frequently used in orthopedics, dentistry [3], drug delivery, cell imaging, and bone tissue engineering [2].

HAp can be produced using chemicals as a source of calcium and phosphates, such as $CaCO_3$ and $H_3PO_4$ [4], $Ca(NO_3)_2$ and $(NH_4)_2HPO_4$ [5], and $Ca(NO_3)_2.4H_2O$ and $KH_2PO_4$ [6]. However, the use of these chemicals is less economical and environmentally friendly, so as a substitute for calcium ion sources, natural sources such as scallop shells [7], blood clam shells [8], eggshells [9], and animal bones [10] are utilized. However, the use of bamboo clam shells has not been widely reported. Bamboo clam shell waste is composed

*Corresponding Author
*Novesar Jamarun, Department of Chemistry, Faculty of Mathematics and Natural Sciences, Universitas Andalas, Padang, 25163, Indonesia.*
*E-mail: novesarjamarun @ sci.unand.ac.id*

of an abundance of calcium (97.58%), so it will be employed in this study as a calcium source [11]. This study will use the precipitation method since it is simple, inexpensive, and produces high-quality yields.

HAP has limited antibacterial activity; therefore, it is necessary to have this property to be applied as a drug carrier. Previous studies have reported the use of ZnO, $TiO_2$, NiO, $SnO_2$, and CdO to provide these antibacterial properties [12–15]. Thus, the present study focuses on the synthesis of HAp/alginate/copper oxide (HAp/Alg/CuO) composite to augment these attributes. An environmentally friendly synthesis approach is explored to synthesize the HAp/Alg/CuO composite. In some previous studies, CuO nanoparticles have been synthesized employing *Averrhoa carambola* leaves extract [16], *Punica granatum* peel extracts [17], *Pterospermum acerifolium* leaves extracts [18], and *Cyperus rotundus* grass extracts [19]. There were no reports on applying *Polyscias scutellaria* leaf extract for synthesizing HAp/Alg/CuO composite. However, Yulizar *et al*. [20] and Yulizar and Ayun [21], have reported the use of *P. scutellaria* and *Polyscias fruticosa* in the synthesis of gold nanoparticles. Figure 1 displays an image of the *P. scutellaria* species.

**Figure 1.** Photograph of *P. scutellaria* species.

*Polyscias scutellaria* leaves contain alkaloids, saponins, flavonoids, and polyphenols, so it is anticipated to function as a capping agent, facilitating control over the composite's morphology [20].

This study was crucial for the preliminary study because the purpose of this study was to synthesize HAp/Alg/CuO composites with outstanding bioactivity, biocompatibility, drug-controlled releases, and antibacterial activity. Next, they can be modified and used for drug delivery systems, especially for clindamycin hydrochloride. Clindamycin hydrochloride (Fig. 2) with IUPAC name of methyl 7-chloro-6,7,8-tri deoxy-6-(1-methyl-trans-4-propyl-L-2-pyrrolidinecarboxamido)-1-thio-L-threo-a-D-galacto-octopyranoside monohydrochloride, is a lincosamide antibiotic that is highly efficient against Gram-positive and Gram-negative anaerobic pathogens [22]. Clindamycin hydrochloride can be used to treat an infection of the bone brought on by pathogenic microorganisms such as the bacteria *Staphylococcus aureus* (*S. aureus*), like osteomyelitis [23].

## MATERIALS AND METHODS

### Materials

Bamboo clam shell, *Sollen* spp. waste and *P. scutellaria* leaves were obtained from Padang, West Sumatera, Indonesia. Alginate impression materials were obtained from Shanghai Medical Instrument, Shanghai, China. Ammonia solution ($NH_4OH$, ≥25%, Merck), diammonium hydrogen phosphate ($(NH_4)_2HPO_4$, ≥99.0%, Merck), nitric acid ($HNO_3$, ≥65%, Merck), copper(II) nitrate trihydrate ($Cu(NO_3)_2.3H_2O$, ≥99.0%, Merck), dimethyl sulfoxide (DMSO, ≥99.7%, Merck), nutrient agar (NA, Merck), and Mueller Hinton agar (MHA, Merck) were purchased from Merck, Darmstadt, Germany. Clindamycin hydrochloride as a drug model for drug delivery assay was obtained from PT. Etercon Pharma, Indonesia.

### Methods

#### *Extraction of P. scutellaria leaf*

The leaves of *P. scutellaria* were collected in Padang, West Sumatra, Indonesia. Phytochemical tests were carried out in the Laboratory of Organic Chemistry and Natural

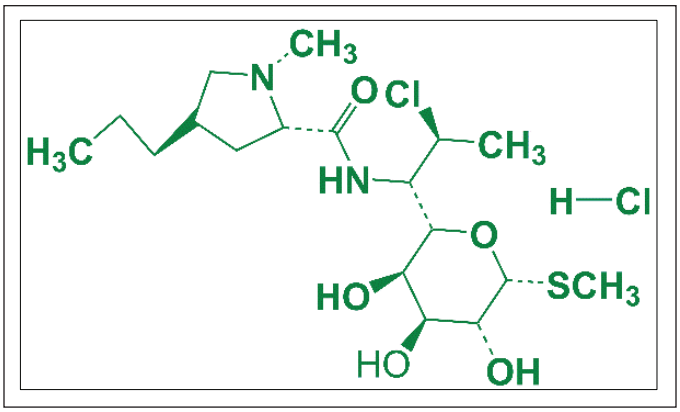


**Figure 2.** Structure of clindamycin hydrochloride.

Materials at Andalas University. The leaves are dried at room temperature for a few days and ground to obtain a fine powder. Ten grams of leaf powder was dispersed into 100 ml of distilled water for 30 minutes at 65°C. The extract was filtered using Whatman filter paper no 41 and then stored in a refrigerator at 4°C.

### *Synthesis of HAp/Alg/CuO composite*

HAp/Alg composite was synthesized by employing a bamboo clam shell as a calcium ion source using the precipitation method based on our previous study [11]. First 1 g of HAp/Alg composite powder was diluted in 50 ml distilled water. Next, copper (II) nitrate trihydrate [Cu $(NO_3)_2.3H_2O$] with mass variations of 0.1, 0.2, 0.3, and 0.4 g, and 1 ml of 4% *P. scutellaria* extract was added to HAp/Alg solution. The temperature during the reaction was set at room temperature. Then, the samples were dried at 110°C for 5 hours and calcined at 600°C for 5 hours to obtain HAp/Alg/CuO composites. The product was labeled as HAp/Alg/CuO-1, HAp/Alg/CuO-2, HAp/Alg/CuO-3, and HAp/Alg/CuO-4. Figure 3 displays the flowchart for synthesizing the HAp/Alg/CuO composite.

### *Instruments*

The structural properties of the HAp/Alg/CuO-1, HAp/Alg/CuO-2, HAp/Alg/CuO-3, and HAp/Alg/CuO-4 samples were analyzed using X-ray diffraction (XRD) (PANalytical, Malvern Panalytical, Malvern, UK) at a $2\theta$ value of 10°–60° with a step size of 0.02. The functional group of the sample was examined using Fourier transform infrared spectroscopy (FTIR) (Perkin Elmer Version 10.6.1, Waltham, MA) at a wavenumber of 4,000–400 $cm^{-1}$. The morphological and elemental compositions of the powder samples were investigated using scanning electron microscopy (SEM) (Hitachi Flexsem 1000, Japan) and energy dispersive spectroscopy (EDS) (Ametek EDAX, Japan) operated at 15 kV.

### *Clindamycin release test*

A solution was prepared by diluting 3 mg of clindamycin hydrochloride and 50 ml of distilled water. The mixture was allowed to react for 2 hours at room temperature. Subsequently, 10 mg of the HAp/Alg/CuO composite powder was introduced into the solution, followed by agitation for 24 hours at a temperature of 37°C. After centrifugation, the mixture was dried at room temperature for 7 days. The clindamycin loaded-HAp/Alg/CuO (CL-HAp/Alg/CuO) samples were dissolved in 50 ml of phosphate-buffered saline (PBS) with a pH of 7.3 and kept on a magnetic stirrer at 100 rpm at 37°C. A total volume of 5 ml was collected from the samples at intervals of 0, 1, 2, 3, 4, 5, and 6 hours. To ensure that the sample volume remained constant at 50 ml, an additional 5 ml of PBS was subsequently introduced. The samples were analyzed using a UV/Vis spectrophotometer set to operate at a wavelength of 210 nm [24]. The total drug release capability of the sample was expressed as a percentage (*t*%).

### *Antibacterial assay*

The well diffusion method assessed the antibacterial activity of CL-HAp/Alg/CuO samples against *Escherichia coli* and *S. aureus* bacteria [25]. First 10 mg/ml of the DMSO solvent was used to dissolve the CL-HAp/Alg/CuO samples. Next, bacterial isolates from NA medium plates were scratched with a sterile ose needle in a zigzag pattern to transfer them to the new NA medium. The NA medium was then cultured with the bacteria for 24 hours. After that, the MHA medium was streaked with the bacterium. Following that, 30 µl of the CL-HAp/Alg/CuO-1, CL-HAp/Alg/CuO-2, CL-HAp/Alg/CuO-3, and CL-HAp/Alg/CuO-4 samples were pipetted into agar wells with a diameter of 7 mm. The Petri dish was maintained at 37°C for 24 hours in an aerobic incubator. The inhibition zone was evaluated following a 24-hour incubation period. Clindamycin HCl and DMSO served as the positive and negative controls, respectively.

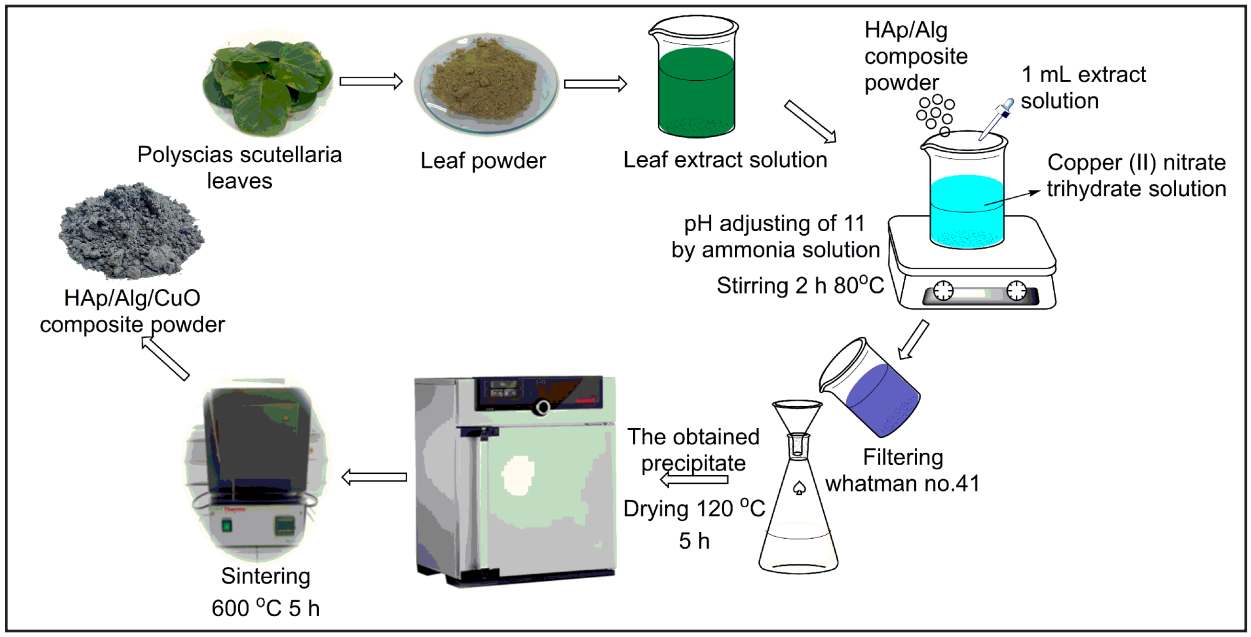


**Figure 3.** The flowchart of the synthesizing HAp/Alg/CuO composite.

## RESULTS AND DISCUSSION

### XRD analysis

The XRD pattern of HAp/Alg/CuO composite at 2$\theta$ 15º–65º is shown in Figure 4a–d. It is possible to discern the distinctive peaks of HAp at 2$\theta$ angles of 25.87º, 32.16º, 46.67º, 49.61º, and 53.22º. Conversely, the peaks of alg are observed at a 2$\theta$ value of 21.82º [11]. The diffraction peaks of CuO were seen at 2$\theta$ angles of 35.64º, 38.74º, 48.44º, and 61.70º. The results are consistent with the hexagonal phase of HAp(ICSD #157481) exhibiting the P 63/m space group [26–28]. Based on the ICDD (The International Centre for Diffraction Data) standard #01-080-1263, it can be observed that the characteristic peak of CuO has a monoclinic structure [16]. Peaks from the three constituent phases consisting of HAp, Alg, and CuO in composing the HAp/Alg/CuO composite indicate that electrostatic interactions between molecules have occurred [29]. The crystallite size was determined using the Scherrer equation

$$D = \frac{k\,\lambda}{\beta\,\mathrm{Cos}\theta}$$

where $k$ is the Scherrer constant (0.89), $\beta$ is the full-width radiants at half maximum of the characteristic diffraction line of Alg, HAp, and CuO, 21.82º, 32.16º, and 35.64º, respectively, $\lambda$ is the wavelength of the Cu-Kα radiation (1.5406 Å), and $\theta$ is the Bragg diffraction [30]. It was obtained at 30.00, 33.35, 24.14, and 26.84 nm for HAp/Alg/CuO-1, HAp/Alg/CuO-2, HAp/Alg/CuO-3, and HAp/Alg/CuO-4, respectively.

### FTIR analysis

The FTIR spectra are depicted in Figure 5 and were acquired within the wavenumber range of 400–4,000 cm$^{-1}$. HAp structure can be inferred from the OH stretching vibrations, which are indicated by the peak observed at 3,435 cm$^{-1}$ [31,32]. The O–P–$Ov_2$ bending vibration is observed at a wavenumber of 472 cm$^{-1}$, while the O–P–$Ov_4$ bending vibration is detected at wavenumbers of 565 and 604 cm$^{-1}$. In addition, the asymmetric stretching of the $PO_4^{3-}$ group is observed at wavenumbers of 1,038 and 1,094 cm$^{-1}$ [33–35]. The vibrational bands seen at 1,633, 1,420, and 793 cm$^{-1}$ correspond to the stretching vibrations of the carboxyl anion from Alg [36]. Meanwhile, the vibrational bands seen at 668 and 732 cm$^{-1}$ correspond to the prominent characteristic bands of the CuO molecule [16]. All absorption bands indicated that the HAp/Alg/CuO composite was synthesized.

### SEM-EDS analysis

SEM images and elemental mapping of the HAp/Alg/CuO-1, HAp/Alg/CuO-2, HAp/Alg/CuO-3, and HAp/Alg/CuO-4 composites were displayed in Figure 6. SEM images depict spherical and irregular-shaped particles with agglomeration. The role of *P. scutellaria* extract as a capping agent was probably not maximized because the volume added was too small so that the particle shape was irregular, with an average particle size of the samples 0.432, 0.390, 0.449, and 0.394 µm for HAp/Alg/CuO-1, HAp/Alg/CuO-2, HAp/Alg/CuO-3, and HAp/Alg/CuO-4, respectively. The EDS spectra exhibited prominent peaks corresponding to calcium, carbon, phosphorus, and oxygen, validating the formation of the HAp/Alg/CuO composite. The elemental mapping analysis further corroborates the results presented in Figure 6. Cu element composition of HAp/Alg/CuO-1, HAp/Alg/CuO-2, HAp/Alg/CuO-3, and HAp/Alg/CuO-4 is 3%, 4%, 5%, and 6%, respectively, according to the increasing CuO concentration in the experiment.

### Clindamycin release

The drug release profiles of the composites are presented in Figure 7. During the initial 2-hour period, the release of clindamycin was determined to be 28.62%, 45.51%, 60%, and 62.41% for HAp/Alg/CuO-1, HAp/Alg/CuO-2, HAp/Alg/CuO-

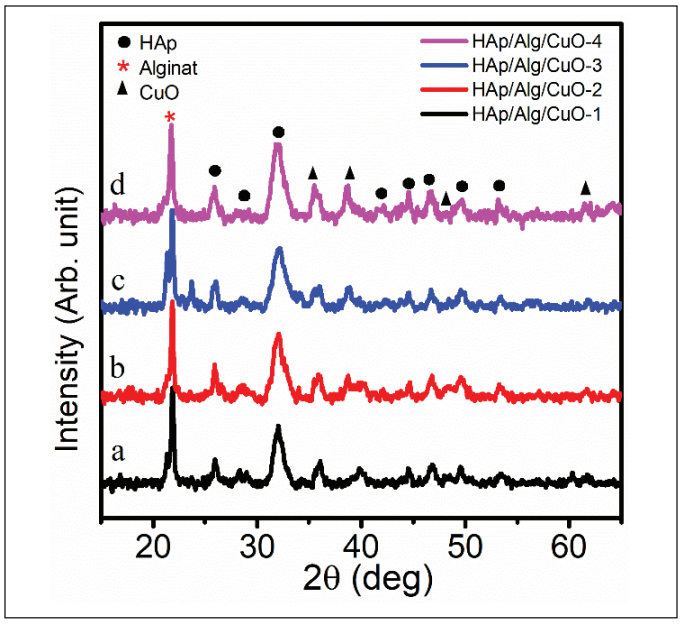


**Figure 4.** XRDs of HAp/Alg/CuO composites: (a) HAp/Alg/CuO-1(black color), (b) HAp/Alg/CuO-2 (red color), (c) HAp/Alg/CuO-3(blue color), and (d) HAp/Alg/CuO-4 (magenta color).

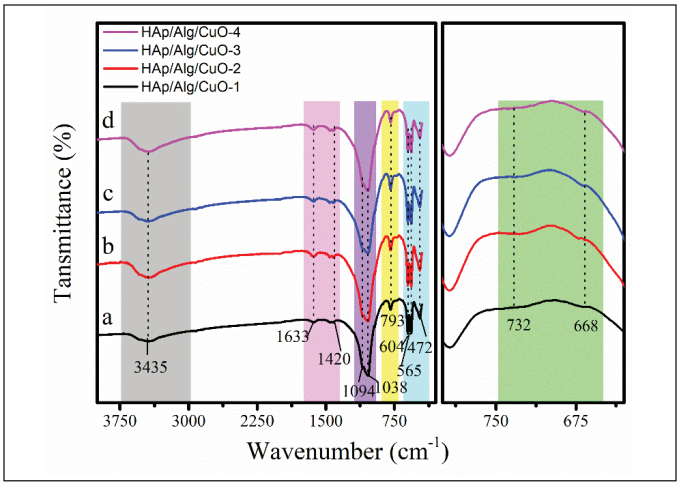


**Figure 5.** FTIR analysis of HAp/Alg/CuO composites: (a) HAp/Alg/CuO-1(black color), (b) HAp/Alg/CuO-2 (red color), (c) HAp/Alg/CuO-3(blue color), and (d) HAp/Alg/CuO-4 (magenta color).

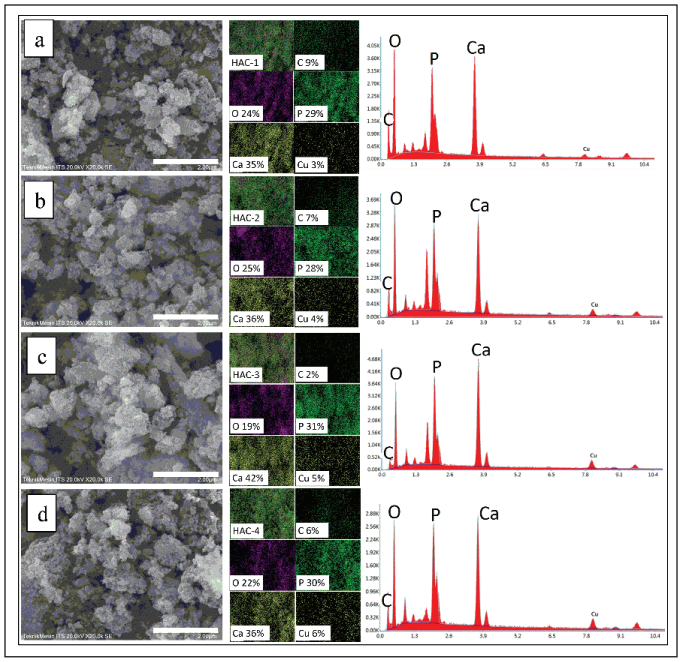


**Figure 6.** Images of SEM (left), mapping (center), and EDS spectra (right) of (a) HAp/Alg/CuO-1, (b) HAp/Alg/CuO-2, (c) HAp/Alg/CuO-3, and (d) HAp/Alg/CuO-4 composites.

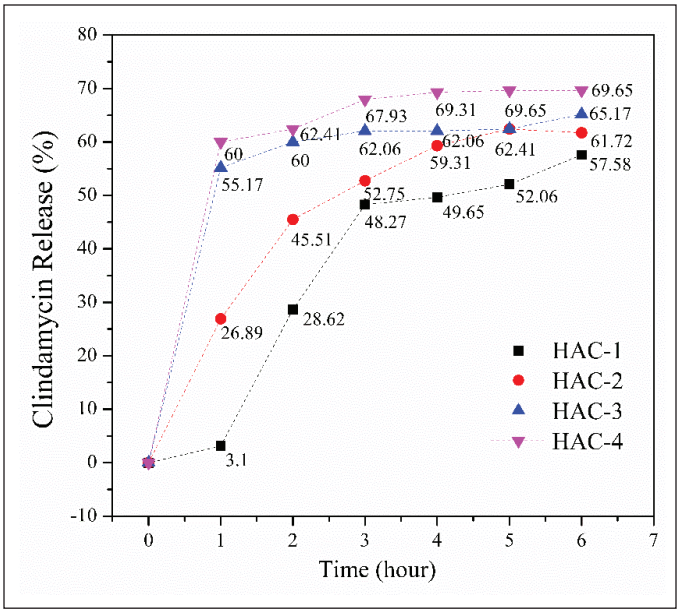


**Figure 7.** Clindamicyn release profile from HAp/Alg/CuO composites, HAp/Alg/CuO-1 (black color), HAp/Alg/CuO-2 (red color), HAp/Alg/CuO-3 (blue color), and HAp/Alg/CuO-4 (magenta color).

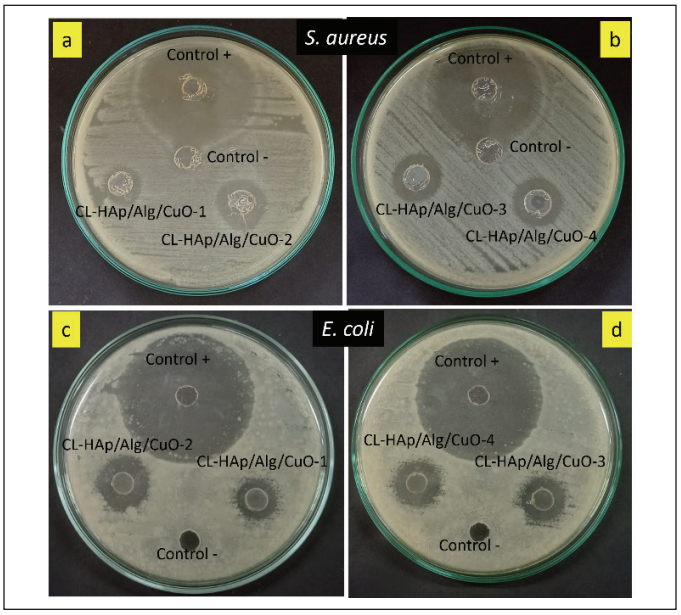


**Figure 8.** Antibacterial assay of CL-HAp/Alg/CuO composites against (a and b) *S. aureus* and (c and d) *E. coli*.

3, and HAp/Alg/CuO-4, respectively. Subsequently, the value mentioned above exhibited an upward trend as time progressed, culminating at the 6-hour mark with respective percentages of 57.58%, 61.72%, 65.17%, and 69.65% for HAp/Alg/CuO-1, HAp/Alg/CuO-2, HAp/Alg/CuO-3, and HAp/Alg/CuO-4. The percentage of drug release that is higher indicates that there is also a higher percentage of drug absorbed [24]. When compared to other composite samples, it can be shown that sample HAp/Alg/CuO-4 exhibits a more controlled drug release. Alginate may be crucial to the efficacy of this composite material since it significantly reduced hydrogel swelling due to a larger degree of cross-linking, delaying the release of the drugs that were contained [37]. CuO in this composite system can help inhibit the growth of bacteria or other microorganisms around the drug delivery site because of its excellent antibacterial properties [38]. This can be useful in treating infections or preventing infections during drug injections; in this case, it is about bone infections due to the *S. aureus* bacteria. The drug release pattern was similar for different concentrations of CuO in the HAp/Alg/CuO composite. In addition, the microstructure, degree of carrier degradation, the medication's solubility, and the nature of interactions between the carrier and the drug all significantly impact how well drug delivery systems operate [23].

### Antibacterial assay

Antibacterial assay of CL-HAp/Alg/CuO composites showed different inhibition zones, as shown in Figure 8. The results showed that *E. coli* and *S. aureus* bacteria were well-grown and distributed on the culture plate, excluding the zone surrounding the wells. The inhibition zone shows that the HAp/Alg/CuO composite can absorb clindamycin, retain it and, resist the bacteria. Excessive use of elemental copper has been shown to be hazardous to aquatic life, humans, animals, and the environment. However, the application of materials based on copper for human use has been approved by the US Environmental Protection Agency, indicating that there is no harm to the biological properties of humans[19].

The inhibition zones are classified into four categories: weak (diameter <5 mm), medium (diameter 5–10 mm), strong (10–20 mm), and very strong (20 mm) [39]. The diameter of the inhibition zone of CL-HAp/Alg/CuO-1, CL-HAp/Alg/

CuO-2, and CL-HAp/Alg/CuO-3 was 6, 8, and 9 mm against *S. aureus* bacteria and 7, 10, and 9 mm against *E. coli* bacteria. Magar *et al*. [14] reported that metal oxide (ZnO) nanoparticles with concentrations of 25, 50, and 100 µg/ml had increased inhibition zones of 8, 10, and 11 mm, respectively. It reveals that CuO has an essential role in presenting antibacterial properties besides the role of clindamycin. The inhibition zone of CL-HAp/Alg/CuO-4 was 10 and 11 mm against *S. aureus* and *E. coli* bacteria, respectively, and these values are the highest among all the composites. Sedefoglu *et al*. [40] also reported that CuO nanoparticles have excellent antibacterial against *S. aureus* bacteria with an inhibition zone of 8 mm for CuO using *Chizopogon roseolus* extract and 11 mm for CuO using *Coprinus comatus* extract. These antibacterial results support the previous clindamycin release test results that CL-HAp/Alg/CuO-4 has the highest percent drug release as well as the largest inhibition zone.

## CONCLUSION

HAp/Alg/CuO composites have been successfully synthesized using the precipitation method and assisted by a green synthesis approach using *P. scutellaria* leaf extract. The results of XRD, FTIR, and SEM-EDS analysis results show that HAp/Alg/CuO composites have been synthesized properly. HAp/Alg/CuO-4 composite had the maximum percentage of drug release, which is 69.65%. This is supported by the antibacterial test, which shows the inhibition zone of CL-HAp/Alg/CuO-4 was 10 and 11 mm against *S. aureus* and *E. coli* bacteria, respectively, and these values are the highest among all the composites. The overall characterization and tests implied that HAp/Alg/CuO composites can be applied for drug carrier materials, especially for clindamycin hydrochloride.

## ACKNOWLEDGMENT

This work was supported by Kementerian Riset dan Teknologi/ Badan Riset dan Inovasi Nasional Republik Indonesia 2022 [grant number T/17/UN.16.17/PT.01.03/PPS-PMDSU-Material Maju/2022] through the PMDSU Scholarship. The author would like to send our gratitude to LPPM (Lembaga Penelitian dan Pengabdian kepada Masyarakat) of Universitas Andalas for supporting the researcher in publishing this work.

## AUTHOR CONTRIBUTIONS

All authors made substantial contributions to the conception and design, acquisition of data, or analysis and interpretation of data; took part in drafting the article or revising it critically for important intellectual content; agreed to submit to the current journal; gave final approval of the version to be published; and agree to be accountable for all aspects of the work. All the authors are eligible to be an author as per the International Committee of Medical Journal Editors (ICMJEs) requirements/guidelines.

## CONFLICTS OF INTEREST

The authors declare no conflicts of interest.

## ETHICAL APPROVALS

This study does not involve experiments on animals or human subjects.

## DATA AVAILABILITY

All data generated and analyzed are included in this research article.

## PUBLISHER'S NOTE

This journal remains neutral with regard to jurisdictional claims in published institutional affiliation.

## REFERENCES

1. Nareswari TL, Juniatik M, Aminatun A, Sari M, Utami RA, Sari YW, *et al.* A facile technique for overcoming seeding barriers of hydrophobic polycaprolactone/hydroxyapatite-based nanofibers for bone tissue engineering. J Appl Pharm Sci. 2023;13(2):49–60. doi: https://doi.org/10.7324/JAPS.2023.130206
2. Ma X, Chen Y, Qian J, Yuan Y, Liu C. Controllable synthesis of spherical hydroxyapatite nanoparticles using inverse microemulsion method. Mater Chem Phys. 2016;183:220–9. doi: https://doi.org/10.1016/j.matchemphys.2016.08.021
3. Saranya K, Kowshik M, Ramanan SR. Synthesis of hydroxyapatite nanopowders by sol-gel emulsion technique. Bull Mater Sci. 2011;34(7):1749–53. doi: https://doi.org/10.1007/s12034-011-0386-8
4. Stanić V, Janaćković D, Dimitrijević S, Tanasković SB, Mitrić M, Pavlović MS, *et al*. Synthesis of antimicrobial monophase silver-doped hydroxyapatite nanopowders for bone tissue engineering. Appl Surf Sci. 2011;257(9):4510–8. doi: https://doi.org/10.1016/j.apsusc.2010.12.113
5. Guo G, Sun Y, Wang Z, Guo H. Preparation of hydroxyapatite nanoparticles by reverse microemulsion. Ceram Int. 2005;31(6):869–72. doi: https://doi.org/10.1016/j.ceramint.2004.10.003
6. Babić B, Đorđevića MP, Maletaškića J, Stankovića N, Yoshidab K, Yanob T, *et al*. *In-situ* immobilization of Sr radioactive isotope using nanocrystalline hydroxyapatite. Ceram Int. 2018;44(2):1771–7. doi: https://doi.org/10.1016/j.ceramint.2018.03.170
7. Islami DM, Wulandari, Jamarun N, Syukri, Sisca V. *In-situ* hydrothermal method for graphene oxide/hydroxyapatite synthesis from scallop shells. Rasayan J Chem. 2023;16(1):456–62. doi: https://doi.org/10.31788/RJC.2023.1618169
8. Azis Y, Jamarun N, Arief S, Nur H. Facile synthesis of hydroxyapatite particles from cockle shells (*Anadara granosa*) by hydrothermal method. Orient J Chem. 2015;31(2):1–7. doi: https://doi.org/10.13005/ojc/310261
9. Sayed M, El-Maghraby HF, Bondioli F, Naga SM. 3D carboxymethyl cellulose/hydroxyapatite (CMC/HA) scaffold composites based on recycled eggshell. J Appl Pharm Sci. 2018;8(3):23–30. doi: https://doi.org/10.7324/JAPS.2018.8304
10. Ramesh S, Loo ZZ, Tan CY, Chew WJK, Ching YC, Tarlochan F, *et al*. Characterization of biogenic hydroxyapatite derived from animal bones for biomedical applications. Ceram Int. 2018;44(9):10525–30. doi: https://doi.org/10.1016/j.ceramint.2018.03.072
11. Wulandari W, Islami DM, Wellia DV, Emriadi E, Sisca V, Jamarun N. The effect of alginate concentration on crystallinity, morphology, and thermal stability properties of hydroxyapatite/alginate composite. Polymers (Basel). 2023;15(3):614. doi: https://doi.org/10.3390/polym15030614
12. Ashpak Shaikh A, Rajendra Patil M, Sonu Jagdale B, Ashok Adole V. Synthesis and characterization of Ag doped ZnO nanomaterial as an effective photocatalyst for photocatalytic degradation of Eriochrome Black T dye and antimicrobial agent. Inorg Chem Commun. 2023;151:110570. doi: https://doi.org/10.1016/j.inoche.2023.110570
13. Waghchaure RH, Adole VA. Biosynthesis of metal and metal oxide nanoparticles using various parts of plants for antibacterial, antifungal and anticancer activity: a review. J Indian Chem Soc. 2023;100(5):100987. doi: https://doi.org/10.1016/j.jics.2023.100987

14. Magar MH, Adole VA, Waghchaure RH, Pawar TB. Efficient photocatalytic degradation of eosin blue dye and antibacterial study using nanostructured zinc oxide and nickel modified zinc oxide. Results Chem 2022;4:100537. doi: https://doi.org/10.1016/j.rechem.2022.100537
15. Uthiram C, Punithavelan N. Efficient magnetic and antibacterial properties of CdO/ZnO nanocomposites prepared via facile hydrothermal method. J King Saud Univ Sci. 2022;34(6):102162. doi: https://doi.org/10.1016/j.jksus.2022.102162
16. Saha T, Bin Mobarak M, Uddin MN, Quddus MS, Naim MR, Pinky NS. Biogenic synthesis of copper oxide (CuO) NPs exploiting *Averrhoa carambola* leaf extract and its potential antibacterial activity. Mater Chem Phys. 2023;305:127979. doi: https://doi.org/10.1016/j.matchemphys.2023.127979
17. Ghidan AY, Al-Antary TM, Awwad AM. Green synthesis of copper oxide nanoparticles using *Punica granatum* peels extract: effect on green peach aphid. Environ Nanotechnol Monit Manag. 2016;6: 95–8. doi: https://doi.org/10.1016/j.enmm.2016.08.002
18. Saif S, Tahir A, Asim T, Chen Y. Plant mediated green synthesis of CuO nanoparticles: comparison of toxicity of engineered and plant mediated CuO nanoparticles towards *Daphnia magna*. Nanomaterials. 2016;6(11):205. doi: https://doi.org/10.3390/nano6110205
19. Suresh S, Ilakiya R, Kalaiyan G, Thambidurai S, Kannan P, Prabu KM, *et al*. Green synthesis of copper oxide nanostructures using *Cynodon dactylon* and *Cyperus rotundus* grass extracts for antibacterial applications. Ceram Int. 2020;46(8):12525–37. doi: https://doi.org/10.1016/j.ceramint.2020.02.015
20. Yulizar Y, Utari T, Ariyanta HA, Maulina D. Green method for synthesis of gold nanoparticles using *Polyscias scutellaria* leaf extract under UV light and their catalytic activity to reduce methylene blue. J Nanomater. 2017;2017:3079636. doi: https://doi.org/10.1155/2017/3079636
21. Yulizar Y, Ayun Q. Bio-prospective of *Polyscias fruticosa* leaf extract as redactor and stabilizer of gold nanoparticles formation. IOP Conf Ser Earth Environ Sci. 2017;60(1):012006. doi: https://doi.org/10.1088/1755-1315/60/1/012006
22. Abushammala IM, El Gussein LA, Zomlot BE, Abushammalleh KF, Taha MM, Miqdad MY. Pharmacokinetic drug-drug interaction study between clindamycin and cyclosporin in rabbits. J Appl Pharm Sci. 2020;10(2):108–11. doi: https://doi.org/10.7324/JAPS.2020.102016
23. Kumar GS, Govindan R, Girija EK. *In situ* synthesis, characterization and *in vitro* studies of ciprofloxacin loaded hydroxyapatite nanoparticles for the treatment of osteomyelitis. J Mater Chem B. 2014;2(31):5052–60. doi: https://doi.org/10.1039/c4tb00339j
24. Tiraton T, Suwantong O, Chuysinuan P, Ekabutr P, Niamlang P, Khampieng T, *et al*. Biodegradable microneedle fabricated from sodium alginate-gelatin for transdermal delivery of clindamycin. Mater Today Commun. 2022;32:104158. doi: https://doi.org/10.1016/j.mtcomm.2022.104158
25. Nigam A, Pawar SJ. Structural, magnetic, and antimicrobial properties of zinc doped magnesium ferrite for drug delivery applications. Ceram Int. 2020;46(4):4058–64. doi: https://doi.org/10.1016/j.ceramint.2019.10.243
26. Abdulkareem MH, Abdalsalam AH, Bohan AJ. Influence of chitosan on the antibacterial activity of composite coating (PEEK /HAp) fabricated by electrophoretic deposition. Prog Org Coatings. 2019;130:251–9. doi: https://doi.org/10.1016/j.porgcoat.2019.01.050
27. Wan F, Ping H, Wang W, Zou Z, Xie H, Su BL, *et al*. Hydroxyapatite-reinforced alginate fibers with bioinspired dually aligned architectures. Carbohydr Polym. 2021;267:118167. doi: https://doi.org/10.1016/j.carbpol.2021.118167
28. Ali A, Hasan A, Negi YS. Effect of carbon based fillers on xylan/chitosan/nano-HAp composite matrix for bone tissue engineering application. Int J Biol Macromol. 2022;197: 1–11. doi: https://doi.org/10.1016/j.ijbiomac.2021.12.012
29. Zheng Y, Wang L, Bai X, Xiao Y, Che J. Bio-inspired composite by hydroxyapatite mineralization on (bis)phosphonate-modified cellulose-alginate scaffold for bone tissue engineering. Colloids Surf A Physicochem Eng Asp. 2022;635:127958. doi: https://doi.org/10.1016/j.colsurfa.2021.127958
30. Prekajski Đorđević M, Maletaškić J, Stanković N, Babić B, Yoshida K, Yano T, *et al*. *In-situ* immobilization of Sr radioactive isotope using nanocrystalline hydroxyapatite. Ceram Int. 2018;44(2):1771–7. doi: https://doi.org/10.1016/j.ceramint.2017.10.110
31. Bera M, Gupta P, Maji PK. Facile one-pot synthesis of graphene oxide by sonication assisted mechanochemical approach and its surface chemistry. J Nanosci Nanotechnol. 2018;18(2):902–12. doi: https://doi.org/10.1166/jnn.2018.14306
32. Victoria EC, Robinson MC. Comparative studies on synthesis and sintering studies of biologically derived hydroxyapatite from *Capria hircus* (Goat) and *Bos primigenius* (Bovine). Vacuum. 2019;160: 378–83. doi: https://doi.org/10.1016/j.vacuum.2018.11.019
33. Sirajudheen P, Karthikeyan P, Vigneshwaran S, Basheer MC, Meenakshi S. Complex interior and surface modified alginate reinforced reduced graphene oxide-hydroxyapatite hybrids: removal of toxic azo dyes from the aqueous solution. Int J Biol Macromol. 2021;175:361–71. doi: https://doi.org/10.1016/j.ijbiomac.2021.02.024
34. Jariya SAI, Padmanabhan VP, Kulandaivelu R, Prakash N, Mohammad F, Al-Lohedan HA, *et al*. Drug delivery and antimicrobial studies of chitosan-alginate based hydroxyapatite bioscaffolds formed by the casein micelle assisted synthesis. Mater Chem Phys. 2021;272:125019. doi: https://doi.org/10.1016/j.matchemphys.2021.125019
35. Laput OA, Zuza DA, Vasenina IV, Savkin KP, Kurzina IA. Effect of silver ION implantation on surface physicochemical properties of composite materials based on polylactic acid and hydroxyapatite. Vacuum. 2020;175:109251. doi: https://doi.org/10.1016/j.vacuum.2020.109251
36. Jain S, Datta M. Montmorillonite-alginate microspheres as a delivery vehicle for oral extended release of venlafaxine hydrochloride. J Drug Deliv Sci Technol. 2016;33:149–56. doi: https://doi.org/10.1016/j.jddst.2016.04.002
37. Sukhodub LF, Sukhodub LB, Litsis O, Prylutskyy Y. Synthesis and characterization of hydroxyapatite-alginate nanostructured composites for the controlled drug release. Mater Chem Phys. 2018;217: 228–34. doi: https://doi.org/10.1016/j.matchemphys.2018.06.071
38. Shinde RS, More RA, Adole VA, Koli PB, Pawar TB, Jagdale BS, *et al*. Design, fabrication, antitubercular, antibacterial, antifungal and antioxidant study of silver doped ZnO and CuO nano candidates: a comparative pharmacological study. Curr Res Green Sustain Chem. 2021;4:100138. doi: https://doi.org/10.1016/j.crgsc.2021.100138
39. Eka Putri G, Arief S, Jamarun N, Gusti FR, Novita Sary A. Characterization of enhanced antibacterial effects of silver loaded cerium oxide catalyst. Orient J Chem. 2018;34:2895–901. doi: https://doi.org/10.13005/ojc/340629
40. Sedefoglu N, Er S, Veryer K, Zalaoglu Y, Bozok F. Green synthesized CuO nanoparticles using macrofungi extracts: characterization, nanofertilizer and antibacterial effects. Mater Chem Phys. 2023;309:128393. doi: https://doi.org/10.1016/j.matchemphys


**How to cite this article:**
Wulandari W, Jamarun N, Wellia DV, Emriadi E. Green precipitation method using *Polyscias scutellaria* extract in the synthesis of hydroxyapatite/alginate/copper (II) oxide composites as a drug carrier. J Appl Pharm Sci. 2024;14(06):147–153.